J. Fluid Mech. (2017), *vol.* 811, *pp.* 612–621.
doi:10.1017/jfm.2016.695

Reverse Marangoni surfing

Vahid Vandadi[1], Saeed Jafari Kang[1] and Hassan Masoud[1,†]

[1]Department of Mechanical Engineering, University of Nevada, Reno, NV 89557, USA

(Received 22 June 2016; revised 15 September 2016; accepted 17 October 2016;
first published online 15 December 2016)

We theoretically study the surfing motion of chemically and thermally active particles located at a flat liquid–gas interface that sits above a liquid layer of finite depth. The particles' activity creates and maintains a surface tension gradient resulting in the auto-surfing. It is intuitively perceived that Marangoni surfers propel towards the direction with a higher surface tension. Remarkably, we find that the surfers may propel in the lower surface tension direction depending on their geometry and proximity to the bottom of the liquid layer. In particular, our analytical calculations for Stokes flow and diffusion-dominated scalar fields (i.e. chemical concentration and temperature fields) indicate that spherical particles undergo reverse Marangoni propulsion under confinement whereas disk-shaped surfers always move in the expected direction. We extend our results by proposing an approximate formula for the propulsion speed of oblate spheroidal particles based on the speeds of spheres and disks.

Key words: interfacial flows (free surface), low-Reynolds-number flows, Marangoni convection

1. Introduction

Self-propelled microdevices powered by converting chemical energy into mechanical work bring to bear functionalities that resemble those of microorganisms. These miniature robots are thus promising candidates for targeted drug delivery, microsurgery, self-assembly and microfluidic manipulation (Sitti 2009; Sitti *et al.* 2015). Thanks to the recent advances in micro/nano technology, researchers have designed and tested a wide variety of swimming microrobots, many of them biomimetic, to carry out prescribed tasks in microfluidic systems (Dreyfus *et al.* 2005; Masoud & Alexeev 2010; Masoud, Bingham & Alexeev 2012; Wang *et al.* 2013; Cheang *et al.* 2014; Duan *et al.* 2015; Maggi *et al.* 2015; Sánchez, Soler & Katuri 2015; Dey *et al.* 2016; Domínguez *et al.* 2016). However, despite recent notable progress in creating microswimmers, the development of microscopic machines capable of surfing on fluidic interfaces is still in its infancy. These tiny surfing robots can potentially execute missions that are currently very difficult, or even impossible, to accomplish.

The motion of a microsurfer is typically driven by a gradient of surface tension, which is prompted by a form of activity taking place at the surface of the surfer (Rayleigh 1889; Nakata *et al.* 1997; Lauga & Davis 2012; Zhao & Pumera 2012; Zhang *et al.* 2013; Masoud & Shelley 2014; Masoud & Stone 2014; Pimienta & Antoine 2014; Würger 2014; Girot *et al.* 2016; Malgaretti, Popescu & Dietrich

† Email address for correspondence: hmasoud@unr.edu

2016). This so-called Marangoni propulsion (Bush & Hu 2006; Lauga & Davis 2012; Masoud & Stone 2014) appears in biological systems as well. For instance, there are water-walking insects that secrete surface-active materials to boost their walking speed in emergency situations (Bush & Hu 2006). A major step towards designing advanced Marangoni-driven microrobots is to establish the relation between the prescribed surface activity and the propulsion velocity in various configurations. A configuration of practical interest involves surfing in the presence of a confining solid boundary.

Here, we theoretically examine the surfing motion of particles located at a flat liquid–gas interface atop a layer of fluid, which is bounded by an impermeable solid wall. We consider chemically and thermally active particles that are, respectively, sources of an insoluble chemical species and heat. The self-induced scalar fields (i.e. concentration of species and temperature fields) locally change the surface tension and the consequent gradients in the surface tension lead to the propulsion of the particle. It is natural to surmise that Marangoni surfers are pulled towards the higher surface tension direction. Contrary to this common instinct, we find that the surfers may propel in the lower surface tension direction depending on their geometry and proximity to the solid wall. Specifically, we show that spherical particles propel in the reverse direction under the confinement whereas disk-shaped surfers always move in the anticipated direction. We rationalize these behaviours in terms of the competition between the effects of the asymmetric surface tension acting along the three-phase contact line and the Marangoni flow engendered by the surface tension gradients. In the following, we first derive closed-form expressions for the translational velocity of spheres and disks. We then extend the results by presenting an approximate expression for the propulsion speed of oblate spheroidal particles based on the speeds of spheres and disks. Overall, our findings pave the way for designing microsurfers capable of operating in bounded environments.

2. Problem formulation and solution

Consider a solid particle located at a flat surface, at $z = 0$, sitting above a layer of Newtonian fluid, with constant viscosity μ, that is bounded by an impermeable solid wall at $z = -H$ (see figure 1). The particle translates with the velocity $\boldsymbol{U} = U\boldsymbol{e}$ due to a non-uniformity in the surface tension γ arising either from the discharge of an insoluble agent (e.g. surfactant) or from the release of heat by the particle. Here, $\boldsymbol{e}$ is the unit vector in the direction of motion.

To reduce the complexity of the analyses, the following (justifiable) assumptions are made: (i) the liquid–gas interface remains flat over distances much greater than the size of the particle, (ii) the three-phase contact line is pinned at a 90° contact angle, (iii) the two-dimensional transport of chemical species and the three-dimensional transport of heat are both dominated by diffusion, (iv) gravitational and inertial effects are negligible, (v) the relevant scalars (i.e. concentration of species and temperature) have linear relations with the surface tension and (vi) the release of the chemical agent and heat are symmetric about the direction of motion, which ensures that the motion of the particle is restricted to translation.

A typical experimental set-up for which the assumptions are valid is an aqueous system with particles of diameter $D \sim 1\,\mu\text{m}$ and propulsion speed $U \sim 1\,\mu\text{m s}^{-1}$ that produce a chemical species with a diffusion constant $\mathcal{D} \sim 10^{-10}\,\text{m}^2\,\text{s}^{-1}$. The capillary, Péclet and Reynolds numbers of this system are, respectively, $Ca = \mu U/\gamma_0 \sim 10^{-8}$, $Pe = DU/\mathcal{D} \sim 10^{-2}$ and $Re = \rho DU/\mu \sim 10^{-6}$. The assumptions are similarly valid

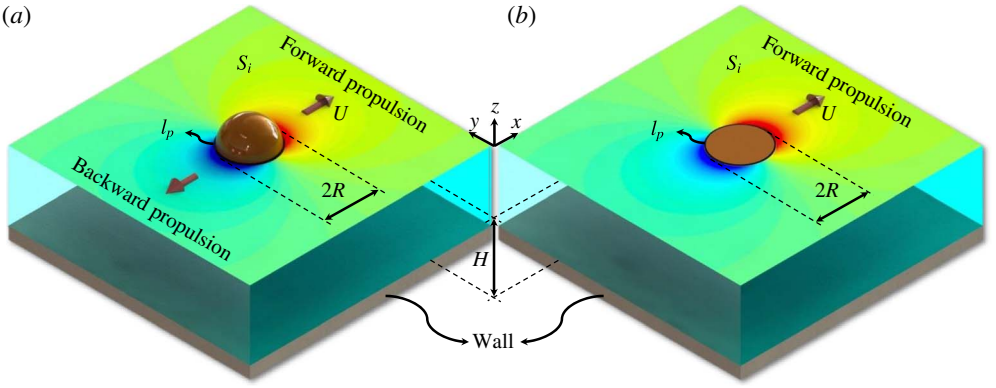

FIGURE 1. (Colour online) Marangoni propulsion of (*a*) spherical and (*b*) disk-shaped particles at a flat interface above a liquid layer of finite depth. The colour maps at the interfaces represent the surface tension distribution stemming either from the discharge of an insoluble agent or from the release of heat by the particle. S_i and l_p denote, respectively, the liquid–gas interface and three-phase contact line pinned to the particle at a 90° contact angle. The translation towards the higher surface tension direction is regarded as the forward propulsion.

for an aqueous system with optically heated particles of diameter $D \sim 10\,\mu\text{m}$ whose propulsion speed is $U \sim 10\,\mu\text{m s}^{-1}$. Here, the corresponding dimensionless numbers are $Ca \sim 10^{-7}$, $Pe = DU/\alpha \sim 10^{-3}$, and $Re \sim 10^{-4}$. The non-dimensional numbers are calculated based on the water properties at room condition (i.e. density $\rho = 997.0479\ \text{kg m}^{-3}$, viscosity $\mu = 8.90 \times 10^{-4}\ \text{N s m}^{-2}$, thermal diffusivity $\alpha = 0.143 \times 10^{-6}\ \text{m}^2\ \text{s}^{-1}$ and surface tension $\gamma_0 = 71.97 \times 10^{-3}\ \text{N m}^{-1}$). In both set-ups, the surface tension is strong enough to keep the interface flat ($Ca \ll 1$), the primary mode of heat and mass transfer is diffusion ($Pe \ll 1$) and the flow is creeping ($Re \ll 1$).

Suppose $\boldsymbol{u}$ and $\boldsymbol{\sigma}$ are, respectively, the velocity and stress fields, in $z \leqslant 0$, corresponding to the Marangoni-driven motion of the particle. Let $\hat{\boldsymbol{u}}$ and $\hat{\boldsymbol{\sigma}}$ denote, respectively, the velocity and stress fields corresponding to the translation with the velocity $\hat{\boldsymbol{U}} = \hat{U}\boldsymbol{e}$ of an identical particle at an interface with no surface tension gradients. These fields are free of contact-line singularities, as the particle motion is limited to pure translation (O'Neill, Ranger & Brenner 1986; Pozrikidis 2007). Hence, according to the Lorentz reciprocal theorem (see Happel & Brenner 1983),

$$\int_{S_p} (\boldsymbol{n}\cdot\boldsymbol{\sigma})\cdot\hat{\boldsymbol{u}}\,\mathrm{d}S + \int_{S_i} (\boldsymbol{n}\cdot\boldsymbol{\sigma})\cdot\hat{\boldsymbol{u}}\,\mathrm{d}S = \int_{S_p} (\boldsymbol{n}\cdot\hat{\boldsymbol{\sigma}})\cdot\boldsymbol{u}\,\mathrm{d}S + \int_{S_i} (\boldsymbol{n}\cdot\hat{\boldsymbol{\sigma}})\cdot\boldsymbol{u}\,\mathrm{d}S, \tag{2.1}$$

where S_p is the wetted area of the particle, S_i represents the liquid–gas interface (see figure 1) and $\boldsymbol{n}$ is the unit vector outward normal to S_p and S_i (see also Masoud & Stone 2014). Integrals over bounding surfaces at infinity are zero since velocities decay at least as fast as the inverse distance in the far field. Integrals over the solid walls also vanish due to the zero-velocity boundary condition.

Owing to the no-slip condition, $\boldsymbol{u} = U\boldsymbol{e}$ and $\hat{\boldsymbol{u}} = \hat{U}\boldsymbol{e}$ on S_p. Also, the components of $\boldsymbol{u}$ and $\hat{\boldsymbol{u}}$ normal to the interface are zero as no fluid exchange takes place there. The balance of shear stress at the interface requires $(\boldsymbol{n}\cdot\boldsymbol{\sigma})\cdot\hat{\boldsymbol{u}} = -\nabla_s\gamma\cdot\hat{\boldsymbol{u}}$ and

$(\boldsymbol{n}\cdot\hat{\boldsymbol{\sigma}})\cdot\boldsymbol{u}=0$ on S_i, where $\boldsymbol{\nabla}_s$ is the surface gradient operator. Since no net external force is applied on the particle, the viscous force $\int_{S_p}\boldsymbol{n}\cdot\boldsymbol{\sigma}\,\mathrm{d}S$ exerted on S_p is balanced by the surface tension force $F_{st}\boldsymbol{e}=\int_{\ell_p}\gamma\boldsymbol{t}\,\mathrm{d}\ell$ acting along the three-phase contact line ℓ_p, where $\boldsymbol{t}$ is the unit vector tangent to S_i and normal to ℓ_p. Taking the above relations into account, (2.1) reduces to

$$U=\frac{\hat{U}}{\hat{F}_d}(F_{st}+F_M), \tag{2.2}$$

where $-\hat{F}_d\boldsymbol{e}=\int_{S_p}\boldsymbol{n}\cdot\hat{\boldsymbol{\sigma}}\,\mathrm{d}S$ is the fluid drag that the translating particle would have experienced in response to its motion at the interface had there been no Marangoni effect and $F_M=\int_{S_i}(\hat{\boldsymbol{u}}/\hat{U})\cdot\boldsymbol{\nabla}_s\gamma\,\mathrm{d}S$ is the contribution of the Marangoni flow.

In the conventional approach, calculating U entails solving the Stokes flow equations for $\boldsymbol{u}$ subject to the no-slip and Marangoni stress boundary conditions (e.g. Lauga & Davis 2012; Würger 2014). The use of the reciprocal theorem, instead, allows us to obtain U by just having $\hat{\boldsymbol{u}}$ (see (2.2)), which is analytically easier to calculate. Conveniently, $\hat{\boldsymbol{u}}$ is already derived for the creeping motion of spherical and disk-shaped particles between parallel plates (Ganatos, Pfeffer & Weinbaum 1980; Davis 1991). Note that when the particle is located at an equal distance from the walls, due to the symmetry, the velocity fields obtained by Ganatos *et al.* (1980) and Davis (1991) are identical to those generated by the translation of the same particle along a flat liquid–gas interface sitting above a liquid layer bounded by a solid boundary. This argument holds when the capillary number is very low, which indicates that the deflection of the interface due to the pressure distribution along the free surface can be ignored. The $Ca\ll 1$ condition is a stronger constraint when the fluid layer is shallow.

Without loss of generality, hereafter, we set the direction of motion to $\boldsymbol{e}=\boldsymbol{e}_x$ (see figure 1). Hence, following the solution of Ganatos *et al.* (1980) for spheres of radius R, the in-plane components of velocity $\hat{\boldsymbol{u}}$ in the spherical coordinates (r,θ,ϕ) at the interface $(\theta=0)$ are

$$\frac{\hat{u}_r}{\hat{U}}=\cos\phi\sum_{m=1}^{\infty}\sum_{n=1}^{3}A_{m,n}(H/R)F_{m,n}(r/R,H/R), \tag{2.3a}$$

$$\frac{\hat{u}_\phi}{\hat{U}}=\sin\phi\sum_{m=1}^{\infty}\sum_{n=1}^{3}A_{m,n}(H/R)G_{m,n}(r/R,H/R), \tag{2.3b}$$

where $\{A_{m,n}\}$ are functions of H/R obtained via a collocation technique and $\{F_{m,n}\}$ and $\{G_{m,n}\}$ are functions of r/R and H/R (see equations (2.6), (2.10), (2.24) and appendix C of Ganatos *et al.* (1980)). Also, according to Davis (1991), the velocity components at $z=0$ in the cylindrical coordinates (r,ϕ,z) for disks of zero thickness and the same radius R are

$$\frac{\hat{u}_r}{\hat{U}}=R^2\cos\phi\left[\frac{\partial}{\partial r}\left(\frac{\Phi_{z,0}}{r}\right)+\frac{\Gamma_0}{r^2}\right], \tag{2.4a}$$

$$\frac{\hat{u}_\phi}{\hat{U}}=R^2\sin\phi\left[-\frac{\Phi_{z,0}}{r^2}-\frac{\partial}{\partial r}\left(\frac{\Gamma_0}{r}\right)\right], \tag{2.4b}$$

where Φ and Γ are functions of r/R, z/R and H/R with $\Gamma_0 = \Gamma|_{z=0}$ and $\Phi_{z,0} = R\,\partial\Phi/\partial z|_{z=0}$ (see equations (4.7), (4.18), (4.19), (4.22) and (4.23) of Davis (1991)).

Following our assumption, the surface tension changes linearly with the concentration of the surface-active agent and the interface temperature as

$$\gamma = \gamma_0 + K_C C + K_T T|_{z=0}, \tag{2.5}$$

where γ_0, K_C and K_T are constants (Acree 1984; Adamson 1990). Here, C and T denote the quasi-steady average-subtracted concentration and temperature fields that satisfy $\nabla_s^2 C = 0$ and $\nabla^2 T = 0$, respectively. This is true when the dominant mechanism of transport is diffusion (i.e. $Pe \ll 1$). Otherwise, advection–diffusion equations for the concentration and temperature fields must be solved simultaneously along with the Stokes equations for the velocity field $\boldsymbol{u}$, in which case the reciprocal theorem no longer provides a shortcut solution.

Inspection of (2.3) and (2.4) reveals that only the first harmonic modes of ϕ appear in $\hat{\boldsymbol{u}}$. This, in conjunction with (2.5), indicates that just the dipolar terms of C and T contribute to the integral in (2.2). Retaining the dipolar parts of their multipole expansions, we can write the concentration and temperature distributions at the interface as

$$C = 2B_C \frac{R\cos\phi}{r} + \cdots, \tag{2.6a}$$

$$T = 2B_T \sum_{n=-\infty}^{\infty} \frac{r\cos\phi}{R\left[(r/R)^2 + (2nH/R)^2\right]^{3/2}} + \cdots, \tag{2.6b}$$

where B_C and B_T are constants. Equation (2.6*b*) is derived using the method of images assuming that both the interface and the solid wall are adiabatic. In case the particles' activity is triggered by a single source point, the value of the dipolar moment is directly related to the off-centre position of the active spot (see e.g. Würger 2014). Remember that since the chemical agent is insoluble in the bulk its concentration C does not depend on the location of the solid wall H.

3. Exact results for spheres and disks

Substituting (2.3)–(2.6) into (2.2), we obtain the propulsion speed for chemically and thermally active spheres and disks. We normalize U by its corresponding value for a semi-infinite fluid layer U_∞ and plot the results as a function of H/R (see figure 2). When the fluid layer is very deep ($H/R \geqslant 100$) the speed is within 2 % of its asymptotic value for all four cases considered, among which chemically and thermally active spheres have, respectively, the slowest and fastest approach rates to U_∞. On the other hand, when the fluid layer is shallow ($H/R < 1.5$), we see distinctly different behaviours for spheres and disks. Notably, we find that spheres come into a halt at a certain distance from the wall ($H/R \simeq 1.25$), closer than which they propel in the lower surface tension direction (see figure 2*a*). This contradicts the default notion that Marangoni surfers self-propel towards the direction with a higher surface tension.

According to (2.2), the sign of U is set by the competition between two opposing influences, namely the net surface tension force acting along the three-phase contact line and the Marangoni flow induced by the surface tension gradients that are represented by F_{st} and F_M, respectively. Note that $\hat{F}_d/\hat{U}$ is always positive (see insets in figure 2). Thus, if the contribution of F_M is neglected, U always has the same sign

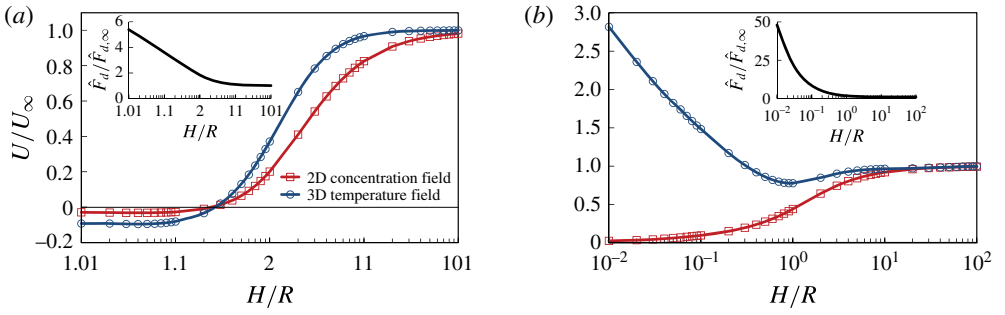

FIGURE 2. (Colour online) The normalized propulsion speed U/U_∞ as a function of the thickness of the fluid layer H/R for (*a*) spherical and (*b*) disk-shaped particles. The squares and circles represent the results for chemically and thermally active particles, respectively. The insets in (*a*) and (*b*) show the variation of $\hat{F}_d/\hat{F}_{d,\infty}$ (normalized Stokes drag experienced by the particle translating at an interface with no surface tension gradients) versus H/R obtained from the solutions of Ganatos *et al.* (1980) and Davis (1991). Here, the speed and drag corresponding to a semi-infinite fluid layer ($H/R \to \infty$) are denoted, respectively, by U_∞ and $\hat{F}_{d,\infty}$, whose values for spheres and disks are shown in figure 3. Also, the thin solid line in (*a*) corresponds to $U = 0$.

as F_{st}, meaning that the particles are always pulled towards the higher surface tension direction. This could be the origin of the common perception about the direction of the Marangoni propulsion.

The effect of the confinement on the propulsion speed of disks is also noteworthy. Figure 2(*b*) shows that U for chemically active disks approaches zero as $H/R \to 0$, whereas, in the same limit, the speed of thermally active disks increases logarithmically. The decay of U in the former can be attributed to the linear rise of $\hat{F}_d$ due to the confinement (see inset in figure 2*b*). The speed surge in the latter however stems from the fact that the solid wall is insulated. The combination of adiabatic condition and narrow layer results in steeper temperature gradients, which further augment F_{st} over F_M. Ultimately, the overall gain of $(F_{st} + F_M)$ outweighs the increase of $\hat{F}_d$ (see figure 2*b* and (2.2)).

Thanks to the reciprocal theorem, we have so far analytically calculated U for spheres and disks. Obtaining U in a similar manner for general oblate spheroids requires a closed-form expression for $\hat{\boldsymbol{u}}$, which is not readily available. In what follows, we propose an approximate method for calculating the propulsion speed of oblate spheroids based on our results for spheres and disks.

4. Approximate results for oblate spheroids

Consider an oblate spheroid translating at an interface above a semi-infinite layer of fluid ($H/R \to \infty$). If we plot the analytically known drag $\hat{F}_{d,\infty}$ as a function of the particle aspect ratio ε (see figure 3*a*), we observe that the drag changes almost linearly with the aspect ratio (see also the Appendix of Stone & Masoud (2015)). In fact, the curve can be approximated extremely well by

$$\hat{F}^D_{d,\infty} + \varepsilon(\hat{F}^S_{d,\infty} - \hat{F}^D_{d,\infty}), \tag{4.1}$$

where the superscripts S and D denote the values for sphere ($\varepsilon = 1$) and disk ($\varepsilon = 0$), respectively. The inset in figure 3(*a*) shows that the maximum relative error is

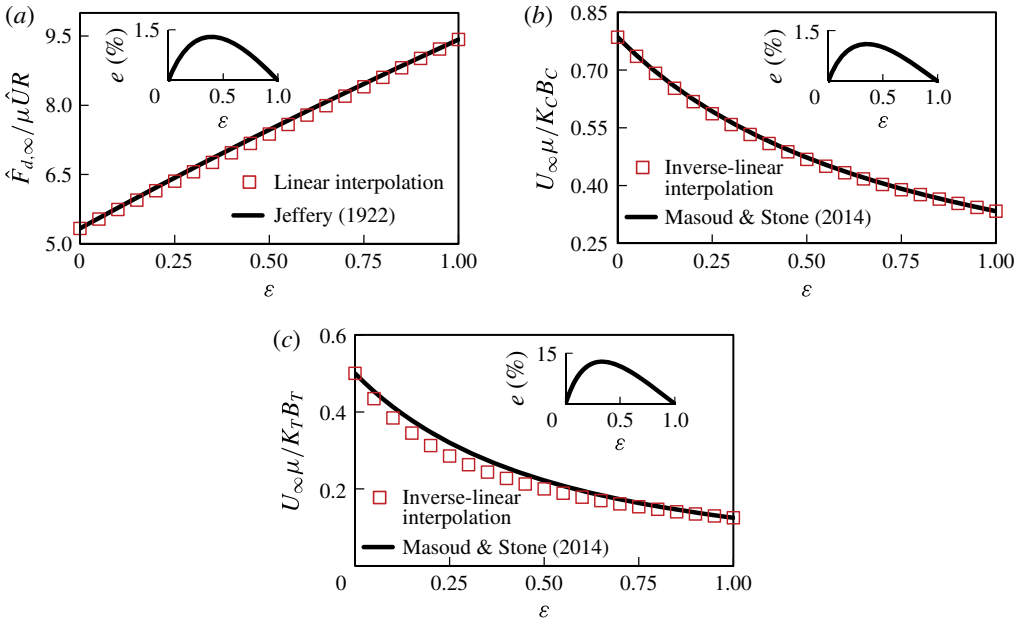

FIGURE 3. (Colour online) Comparison between the exact and approximate results for oblate spheroidal particles translating at an interface above a semi-infinite layer of fluid ($H/R \to \infty$). (*a*) The variation of non-dimensional drag $\hat{F}_{d,\infty}/\mu\hat{U}R$ versus the particle aspect ratio ε. The dimensionless propulsion speed of (*b*) chemically and (*c*) thermally active spheroids (respectively, $U_\infty\mu/K_CB_C$ and $U_\infty\mu/K_TB_T$) as a function of ε. The solid lines represent exact analytical results whereas square symbols depict approximate values obtained via interpolations between the results for spheres and disks. The insets show the relative error of the approximations.

1.3 % belonging to $\varepsilon = 0.4$. That the particle resistance varies quasi-linearly with the aspect ratio suggests that the particle mobility (e.g. U) changes inverse linearly with ε. Remarkably, we find that the curves of U_∞ versus ε for chemically and thermally active spheroids are closely represented by (see figures 3*b* and 3*c*)

$$\left[\frac{1}{U_\infty^D} + \varepsilon\left(\frac{1}{U_\infty^S} - \frac{1}{U_\infty^D}\right)\right]^{-1}. \tag{4.2}$$

Again, the maximum error occurs at $\varepsilon = 0.4$ and its magnitude is 1.1 % and 12.5 % for chemically and thermally active particles, respectively (see insets of figures 3*b* and 3*c*).

These observations strongly recommend employing the same type of interpolations used in (4.1) and (4.2) for approximating the drag $\hat{F}_d$ and propulsion speed U of oblate spheroidal particles in the presence of the confining solid boundary. To test the validity of such estimations, we numerically calculate $\hat{F}_d$ and U for $\varepsilon = 0.4$ and compare the results with those obtained by interpolating between the data presented in figure 2. Our numerical approach integrates a boundary singularity method with the (infinite) image technique (Blake 1971). Also, we choose $\varepsilon = 0.4$ because, very likely, the error is maximum at this aspect ratio (see insets of figure 3). Indeed, we find that the approximations for U are reasonably accurate, particularly for $H/R \geqslant 4$

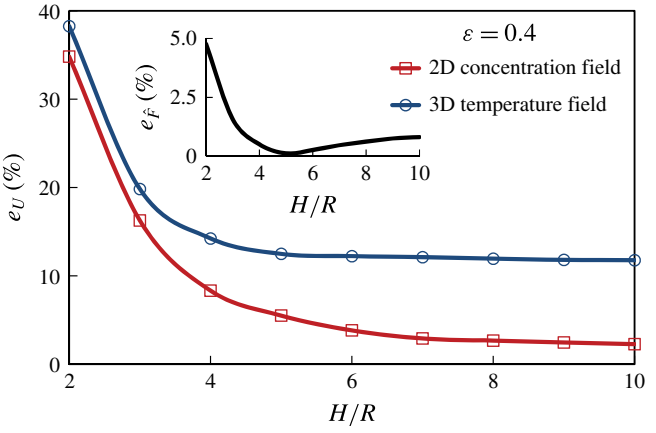

FIGURE 4. (Colour online) Comparison between the numerical and approximate results for oblate spheroidal particles of aspect ratio $\varepsilon = 0.4$. The squares and circles, respectively, represent the relative approximation error e_U for the propulsion speed of chemically and thermally active particles at different distances from the wall H/R. The inset shows the relative error for the drag $e_{\hat{F}}$ as a function of H/R.

(see figure 4). The interpolation performs even better for $\hat{F}_d$, where the error is below 5 % for $H/R \geqslant 2$.

5. Conclusions

We theoretically examined the effect of confinement on the Marangoni propulsion of oblate spheroidal particles. We demonstrated that, depending on the geometry and degree of confinement, the surfing particles may propel forward in the higher surface tension direction or propel backward in the reverse direction. Knowing that the direction of propulsion is altered by a change in the surrounding boundary can be harnessed for designing smart surfing robots capable of sensing their environment.

In this work, we only considered particles with a 90° contact angle (i.e. half-submerged). However, the propulsion speed of a particle with a contact angle other than 90° can be estimated by calculating the speed of a half-submerged oblate spheroid with the same protrusion length to the liquid phase and the same contact-line radius. It has been shown that the fluid drags experienced by the two particles are closely comparable (see e.g. Stone & Masoud 2015).

Lastly, while our findings shed new light on the geometry–speed relation for Marangoni surfers, they also open up new questions such as how does the competition between the net surface tension force and the Marangoni flow generated by the surface tension gradients play itself out when the inertia is important, when the transport of the scalars is no longer dominated by diffusion or when the interface is curved? Answering these and other relevant questions will be the subject of future studies. It will also be interesting to see whether there exist examples of the reverse Marangoni propulsion in natural or biological systems.

Acknowledgements

We thank H. A. Stone for stimulating discussions. Partial support from the Nevada Advanced Autonomous Systems Innovation Center (NAASIC) is also acknowledged.

REFERENCES

ACREE, W. E. 1984 Empirical expression for predicting surface-tension of liquid-mixtures. *J. Colloid Interface Sci.* **101**, 575–576.

ADAMSON, A. W. 1990 *Physical Chemistry of Surfaces*. Wiley.

BLAKE, J. R. 1971 A note on the image system for a Stokeslet in a no-slip boundary. *Math. Proc. Cambridge* **70** (02), 303–310.

BUSH, J. W. M. & HU, D. L. 2006 Walking on water: biolocomotion at the interface. *Annu. Rev. Fluid Mech.* **38**, 339–369.

CHEANG, U. K., MESHKATI, F., KIM, D., KIM, M. J. & FU, H. C. 2014 Minimal geometric requirements for micropropulsion via magnetic rotation. *Phys. Rev.* E **90** (3), 033007.

DAVIS, A. M. J. 1991 Slow viscous flow due to motion of an annular disk; pressure-driven extrusion through an annular hole in a wall. *J. Fluid Mech.* **231**, 51–71.

DEY, K. K., WONG, F., ALTEMOSE, A. & SEN, A. 2016 Catalytic motors–Quo Vadimus? *Curr. Opin. Colloid Interface Sci.* **21**, 4–13.

DOMÍNGUEZ, A., MALGARETTI, P., POPESCU, M. N. & DIETRICH, S. 2016 Effective interaction between active colloids and fluid interfaces induced by Marangoni flows. *Phys. Rev. Lett.* **116**, 078301.

DREYFUS, R., BAUDRY, J., ROPER, M. L., FERMIGIER, M., STONE, H. A. & BIBETTE, J. 2005 Microscopic artificial swimmers. *Nature* **437** (7060), 862–865.

DUAN, W., WANG, W., DAS, S., YADAV, V., MALLOUK, T. E. & SEN, A. 2015 Synthetic nano-and micromachines in analytical chemistry: sensing, migration, capture, delivery, and separation. *Annu. Rev. Anal. Chem.* **8**, 311–333.

GANATOS, P., PFEFFER, R. & WEINBAUM, S. 1980 A strong interaction theory for the creeping motion of a sphere between plane parallel boundaries. Part 2. Parallel motion. *J. Fluid Mech.* **99** (04), 755–783.

GIROT, A., DANNÉ, N., WÜRGER, A., BICKEL, T., REN, F., LOUDET, J. C. & POULIGNY, B. 2016 Motion of optically heated spheres at the water-air interface. *Langmuir* **32** (11), 2687–2697.

HAPPEL, J. & BRENNER, H. 1983 *Low Reynolds Number Hydrodynamics, with Special Applications to Particulate Media*. Prentice-Hall.

LAUGA, E. & DAVIS, A. M. J. 2012 Viscous Marangoni propulsion. *J. Fluid Mech.* **705**, 120–133.

MAGGI, C., SAGLIMBENI, F., DIPALO, M., DE ANGELIS, F. & DI LEONARDO, R. 2015 Micromotors with asymmetric shape that efficiently convert light into work by thermocapillary effects. *Nat. Commun.* **6**, 7855.

MALGARETTI, P., POPESCU, M. N. & DIETRICH, S. 2016 Active colloids at fluid interfaces. *Soft Matt.* **12**, 4007–4023.

MASOUD, H. & ALEXEEV, A. 2010 Modeling magnetic microcapsules that crawl in microchannels. *Soft Matt.* **6** (4), 794–799.

MASOUD, H., BINGHAM, B. I. & ALEXEEV, A. 2012 Designing maneuverable micro-swimmers actuated by responsive gel. *Soft Matt.* **8** (34), 8944–8951.

MASOUD, H. & SHELLEY, M. J. 2014 Collective surfing of chemically active particles. *Phys. Rev. Lett.* **112**, 128304.

MASOUD, H. & STONE, H. A. 2014 A reciprocal theorem for Marangoni propulsion. *J. Fluid Mech.* **741**, R4.

NAKATA, S., IGUCHI, Y., OSE, S., KUBOYAMA, M., ISHII, T. & YOSHIKAWA, K. 1997 Self-rotation of a camphor scraping on water: new insight into the old problem. *Langmuir* **13** (16), 4454–4458.

O'NEILL, M. E., RANGER, K. B. & BRENNER, H. 1986 Slip at the surface of a translating–rotating sphere bisected by a free surface bounding a semi-infinite viscous fluid: removal of the contact-line singularity. *Phys. Fluids* **29** (4), 913–924.

PIMIENTA, V. & ANTOINE, C. 2014 Self-propulsion on liquid surfaces. *Curr. Opin. Colloid Interface Sci.* **19** (4), 290–299.

POZRIKIDIS, C. 2007 Particle motion near and inside an interface. *J. Fluid Mech.* **575**, 333–357.

RAYLEIGH, LORD 1889 Measurements of the amount of oil necessary in order to check the motions of camphor upon water. *Proc. R. Soc. Lond.* **47** (286–291), 364–367.

SÁNCHEZ, S., SOLER, L. & KATURI, J. 2015 Chemically powered micro-and nanomotors. *Angew. Chem. Intl Ed. Engl.* **54** (5), 1414–1444.

SITTI, M. 2009 Miniature devices: voyage of the microrobots. *Nature* **458** (7242), 1121–1122.

SITTI, M., CEYLAN, H., HU, W., GILTINAN, J., TURAN, M., YIM, S. & DILLER, E. 2015 Biomedical applications of untethered mobile milli/microrobots. *Proc. IEEE* **103** (2), 205–224.

STONE, H. A. & MASOUD, H. 2015 Mobility of membrane-trapped particles. *J. Fluid Mech.* **781**, 494–505.

WANG, W., DUAN, W., AHMED, S., MALLOUK, T. E. & SEN, A. 2013 Small power: autonomous nano-and micromotors propelled by self-generated gradients. *Nano Today* **8** (5), 531–554.

WÜRGER, A. 2014 Thermally driven Marangoni surfers. *J. Fluid Mech.* **752**, 589–601.

ZHANG, H., DUAN, W., LIU, L. & SEN, A. 2013 Depolymerization-powered autonomous motors using biocompatible fuel. *J. Am. Chem. Soc.* **135** (42), 15734–15737.

ZHAO, G. & PUMERA, M. 2012 Liquid–liquid interface motion of a capsule motor powered by the interlayer Marangoni effect. *J. Phys. Chem.* B **116** (35), 10960–10963.